Journal of Membrane Science 452 (2014) 379–389

Contents lists available at ScienceDirect

Journal of Membrane Science

journal homepage: www.elsevier.com/locate/memsci

Novel method for incorporating hydrophobic silica nanoparticles on polyetherimide hollow fiber membranes for CO_2 absorption in a gas–liquid membrane contactor

Yuan Zhang [a,b], Rong Wang [a,b,*]

[a] School of Civil and Environmental Engineering, Nanyang Technological University, 50 Nanyang Avenue, Singapore 639798, Singapore
[b] Singapore Membrane Technology Centre, Nanyang Environment and Water Research Institute, Nanyang Technological University, 1 Cleantech Loop, Singapore 637141, Singapore

ARTICLE INFO

Article history:
Received 11 June 2013
Received in revised form
3 October 2013
Accepted 6 October 2013
Available online 22 October 2013

Keywords:
PEI hollow fiber membranes
Fluorinated silica
Composite membranes
Hydrophobicity
Gas–liquid membrane contactor

ABSTRACT

In a gas–liquid membrane contactor, a larger pore size can result in a lower membrane mass transfer resistance. However, the membrane pore size is usually limited by the concern of pore wetting, e.g. a large pore size means a higher wetting tendency. As a breakthrough, this paper reported a porous polyetherimide (PEI) hollow fiber membrane with high surface porosity and large pore size to minimize the membrane mass transfer resistance by using a triple-orifice spinneret in the hollow fiber spinning process, and followed by a novel approach of fluorinated silica ($fSiO_2$) nanoparticles (NPs) incorporation to make the membrane surface highly hydrophobic and chemical resistant to prevent the membrane from wetting caused by the large pore size on the membrane surface. The newly developed composite hollow fiber membranes showed the advancing contact angle value of 123.3°, receding contact angle value of 107.2°, and contact angle hysteresis of only 15.9°, indicating the high water resistant property. The composite membrane also exhibited a higher rigidity property compared with the original PEI substrate. The CO_2 absorption flux of the composite membranes was investigated in both physical and chemical absorptions in a gas–liquid membrane contactor system. The membrane contactor showed a stable performance throughout the 60 d long-term operation using a 2 M sodium taurinate aqueous solution as the liquid absorbent.

The highly hydrophobic composite hollow fiber membrane was able to outperform a conventional polymeric hydrophobic membrane in term of superior gas absorption flux and outstanding long-term stability, suggesting that the formation of organic–inorganic composite membranes is an effective way to enhance the feasibility of membrane contactor processes for practical applications. The results demonstrated the important role of membrane fabrication and modification techniques in facilitating the commercialization of membrane contactor technology.

1. Introduction

Membrane contactor technology, which integrates the acid gas absorption process with the membranes, is increasingly seen as a promising alternative in past decades for CO_2 capture. In a gas–liquid membrane contactor, the gas stream and liquid solution flow on different sides of the membrane, the target gas can transport through the microporous membrane and being absorbed by the liquid absorbent. The membrane serves as an interfacial barrier between the gas and liquid phase, thus the membrane is non-selective and able to minimize the mass transfer resistance posed by the membrane phase. Overall, the gas–liquid membrane contactor offers several advantages over the conventional devices: (1) high surface area per unit volume and less energy-consuming so that it is more economic; (2) the gas and liquid phases flow independently at the different sides of the membrane (lumen and shell), and hence can be manipulated separately; (3) the compact modular structure provides the flexibility for scale up or down; and (4) the interfacial area is known and independent to the operational conditions so that the system performance can be predicted easily [1,2].

Commonly used hydrophobic materials include polytetrafluoroethylene (PTFE), polypropylene (PP), polyethylene (PE), and polyvinylidene fluoride (PVDF) as well as the co-polymer of poly (vinylidene fluoride-co-hexafluropropylene) (PVDF-HFP). Except for the PTFE membrane, however, most of the hydrophobic membranes are not able to maintain long-term absorption

* Corresponding author at: School of Civil and Environmental Engineering, Nanyang Technological University, 50 Nanyang Avenue, Singapore 639798, Singapore. Tel.: +65 6790 5327; fax: +65 6791 0676.
E-mail address: rwang@ntu.edu.sg (R. Wang).

0376-7388/$ - see front matter © 2013 Elsevier B.V. All rights reserved.
http://dx.doi.org/10.1016/j.memsci.2013.10.011

performance due to either larger pore sizes or less hydrophobicity caused by the chemical attacks of the absorbents used [3–5]. Therefore, the development of highly hydrophobic and chemical resistant membranes with an optimized substrate structure to avoid wetting has become a critical issue to facilitate membrane contactor practical application in CO_2 separation.

The essential properties of the membranes for contactor applications include: high hydrophobicity, high surface porosity, low mass transfer resistance and resistance to the chemical liquid absorbents [6]. An asymmetric hollow fiber membrane prepared from the NIPS process usually exhibits a dense skin layer and porous substrate. The most mass transfer resistance in the membrane comes from the dense skin layer, while the porous substrate only provides mechanical support and fractional resistance. The pore size and pore size distribution of the skin layer significantly affect the CO_2 absorption flux and membrane wetting problem since the skin layer is in direct contact with the liquid absorbents. Atchariyawut et al. reported that the ratio of the membrane resistance over the overall mass transfer resistance increased with skin layer pore sizes [7].

On the other hand, according to the Young–Laplace equation [8,9] as shown in Eq. (1), with increase in the pore size, the liquid entry pressure decreases, indicating higher membrane wettability

$$\Delta p = \frac{4\sigma_l \cos\theta}{d_{max}} \quad (1)$$

where σ_l is the liquid surface tension, θ is the contact angle between the liquid and membrane surface, and d_{max} is the maximum pore diameter in the microporous membrane. It can be seen that the factors affecting the value of breakthrough pressure are liquid surface tension, membranes hydrophobicity and the maximum membrane pore size. A high liquid entry pressure requires the membrane as hydrophobic as possible with a small pore size and narrow pore size distribution. Increase in membrane pore size would have an adverse effect in liquid resistant property of the membrane. Thus, the pore size is always limited by the concern of membrane wettability when fabricating the membranes for contactor applications. Herein, to make the breakthrough, we are going to report a porous PEI substrate with high surface porosity and large pore size to minimize the membrane mass transfer resistance by using a triple-orifice spinneret in the hollow fiber spinning process, and followed by a novel approach of hydrophobic inorganic nanoparticles (NPs) incorporation to make the membrane surface highly hydrophobic and chemical resistant to prevent the membrane from wetting caused by the large pore size on the membrane surface.

In recent years, a triple-orifice spinneret has been developed mainly for fabricating dual layer hollow fiber membranes [10–12]. Basically, the bore fluid, the first dope solution and the second dope solution as the external liquid were pumped through the inner, middle and outer channels of the spinneret, respectively. It has been reported that solvent can also be used as the external liquid, flowing in the outer channel of the triple-orifice spinneret, and extruded simultaneously with the dope solution and bore fluid in the spinning process [13,14]. He et al. were the first used this approach to fabricate porous polysulfone (PSf) with N-Methyl-2-Pyrrolidone (NMP) as the external liquid at the outside orifice of the spinneret [13]. It was found that the resultant membranes had a highly open and porous outer skin. Later, Bonyadi et al. reported a highly porous and macrovoids-free PVDF hollow fiber membrane by using the same approach for membrane distillation (MD) application and an improved MD flux was observed [14].

In this study, we used this approach to fabricate the PEI hollow fiber membrane with high surface porosity and pore size. After obtaining the good substrate, the incorporation of fluorinated silica ($fSiO_2$) NPs on the membrane surface were conducted. Nanostructured architecture with highly hydrophobic fluorocompounds were imparted on the membrane surface and resulted in a highly rough and hydrophobic membrane surface. In the previous study [15], we have successfully fabricated novel PEI-$fSiO_2$ composite hollow fiber membranes for membrane contactor application. In this study, we further improved the properties of the composite membranes and CO_2 absorption performance in the membrane contactor by optimizing the PEI substrate structure and improving the approach for $fSiO_2$ NP incorporation. The formation of the composite membranes was examined by attenuated total reflectance-fourier transform infrared spectroscopy (ATR-FTIR). The membrane morphologies were observed by a scanning electron microscope (SEM) and analyzed by atomic force microscopy (AFM). Surface hydrophobicity and mechanical properties of the composite membranes were also investigated. The CO_2 absorption performance of the composite membranes was evaluated in both physical and chemical absorptions in a gas–liquid membrane contactor system. A long-term performance test of the composite membrane in membrane contactor was carried out for 60 d.

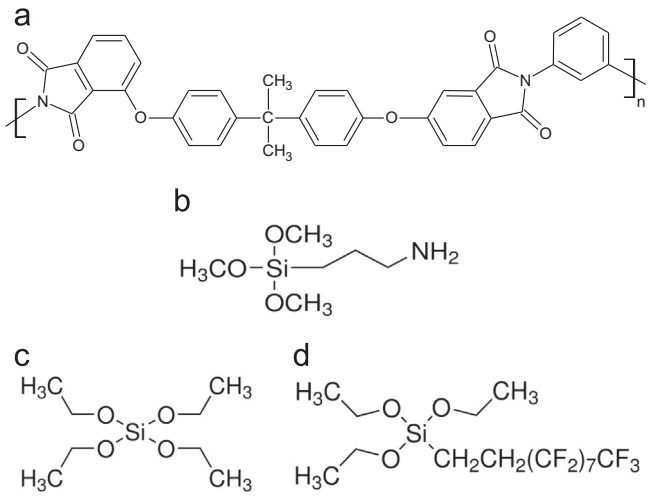

Fig. 1. Chemical structure of (a) Ultem®1000; (b) APTMS; (c) TEOS; and (d) PFTS.

2. Experimental

2.1. Materials

The membrane material, polymer PEI, commercially known as Ultem®1000, was purchased from GE. NMP (> 99.5%, CAS#872-50-4, Merck) was used as a solvent. Lithium chloride (LiCl, anhydrous, CAS#7447-41-8, MP Biomed) was used as the membrane pore former. (3-Aminopropy) trimethoxysilane (APTMS, 97%, CAS#13822-56-5, Aldrich), tetraethyl orthosilicate (TEOS, ≥ 99%, CAS#78-10-4, Merck) and 1H, 1H, 2H, 2H-perfluorodecyltriethoxysilane (PFTS, 97%, CAS#101947-16-4, Aldrich) were used. Iso-propanol (IPA, 99.9%, CAS#67-63-0, Merck), ammonium (26% $NH_3 \cdot H_2O$, Merck), ethanol (CAS#64-17-5, Merck) and n-hexane (CAS#110-54-3, Merck) were used for preparing the solutions. Milli-Q deionized water was used in all aqueous solutions (18 MΩ cm). Taurine ($C_2H_7NO_3S$, 99%, CAS#107-35-7, Acros) and sodium hydroxide (NaOH, CAS#1310-73-2, Merck) were used to prepare the 2 M sodium taurinate solution as the CO_2 absorbent used in the membrane contactor. All the reagents were used as received. The chemical structures of Ultem®1000, APTMS, TEOS and PFTS are given in Fig. 1.

2.2. PEI membrane preparation

The PEI asymmetric hollow fiber membrane substrates were fabricated by a dry-jet wet spinning process using the spinning system. The polymer dope solution was prepared by dissolving the

pre-dried PEI polymer powder and LiCl as pore former with desired amounts in NMP solvent at the temperature of 333.15 K for 3 d. The homogenous dope solution was then cooled down to room temperature and subsequently degassed under vacuum for overnight before spinning. In the spinning process, the solvent, dope and bore fluid were extruded through the outer, middle and inner channel of the spinneret at a controlled rate and went through an air gap before immersing into a coagulation bath. Tap water was used as the external coagulant whilst the mixtures of Milli-Q water and NMP were used as the bore fluid. The nascent hollow fibers were collected at free-falling take-up speed and subsequently stored in a water bath for at least 2 d to remove residual solvents. The spinning conditions were summarized in Table 1.

2.3. Formation of the composite membrane

The PEI substrates were firstly treated by APTMS solution so that the silanol groups can be imparted on the membrane surface. The detailed procedure of APTMS treatment can be found in our previous work in Zhang et al. [15]. The SiO_2 precursor solution was prepared based on the well-known Stober method [16]. Briefly, a 20 ml TEOS were dissolved in a 100 ml ethanol solution and mixed well. The solution was added dropwise to another solution containing 24 ml ammonium in a 100 ml ethanol with agitation. The mixture was stirred intensively at room temperature. After stirring for 12 h, the mixture was treated by probe ultrasonication for 20 min to alleviate the SiO_2 NPs aggregation in the solution. The APTMS treated PEI membranes were immersed in the above solution for 2 h with shaking. The hydroxyl groups on the membrane surface reacted with SiO_2 NPs through condensation reaction. Subsequently, the membranes were rinsed with abundant ethanol to remove loosely bonded and stacked layer of SiO_2 NPs on the membrane surface and placed in an oven at 373.15 K for 1 h. Herein, the PEI substrate with nanostructured SiO_2 hydrophilic surface was obtained. To get the nanostructured hydrophobic surface, the membranes were further hydrophobically treated by a 2 wt% PFTS in n-hexane at room temperature for 2 h. The PFTS molecules were opt to react with the hydroxide groups on the membrane surface. The membranes were then dried in oven at 373.15 K for 1 h. The final composite membranes were designated as PEI-fSiO_2. The reaction route and mechanism of the formation of the PEI-fSiO_2 composite membrane is schematically presented in Figs. 2 and 3, respectively. In our previous work [15], fluorination was done in a single step by mixing TEOS and PFTS together to allow the hydrolysis, polycondensation and fluorination reactions occur simultaneously to generate fSiO_2 particles in the solution. In this study, fluorination as the final treatment step was favorable to generate a more uniform coverage of PFTS network on the SiO_2 layer surface.

Table 1
Spinning parameters for fabricating PEI hollow fiber substrates.

Parameters	PEI
Dope composition (wt%)	PEI/LiCl/NMP (14/3/83)
Dope flow rate (g/min)	3.78
Outer channel solvent	PEI A: – PEI B: NMP
Solvent flow rate (ml/min)	PEI A: – PEI B: 1
Bore fluid (wt%)	DI water/NMP (20/80)
Bore fluid flow rate (ml/min)	3
Length of air gap (cm)	5
Take up speed	Free fall
External coagulant	Water
Spinning temperature	298.15 K

2.4. Membrane characterizations

2.4.1. Membrane morphology observation

The membrane samples were observed by the Scanning Electron Microscope (SEM, JSM-7600F JOEL) at an operating voltage of

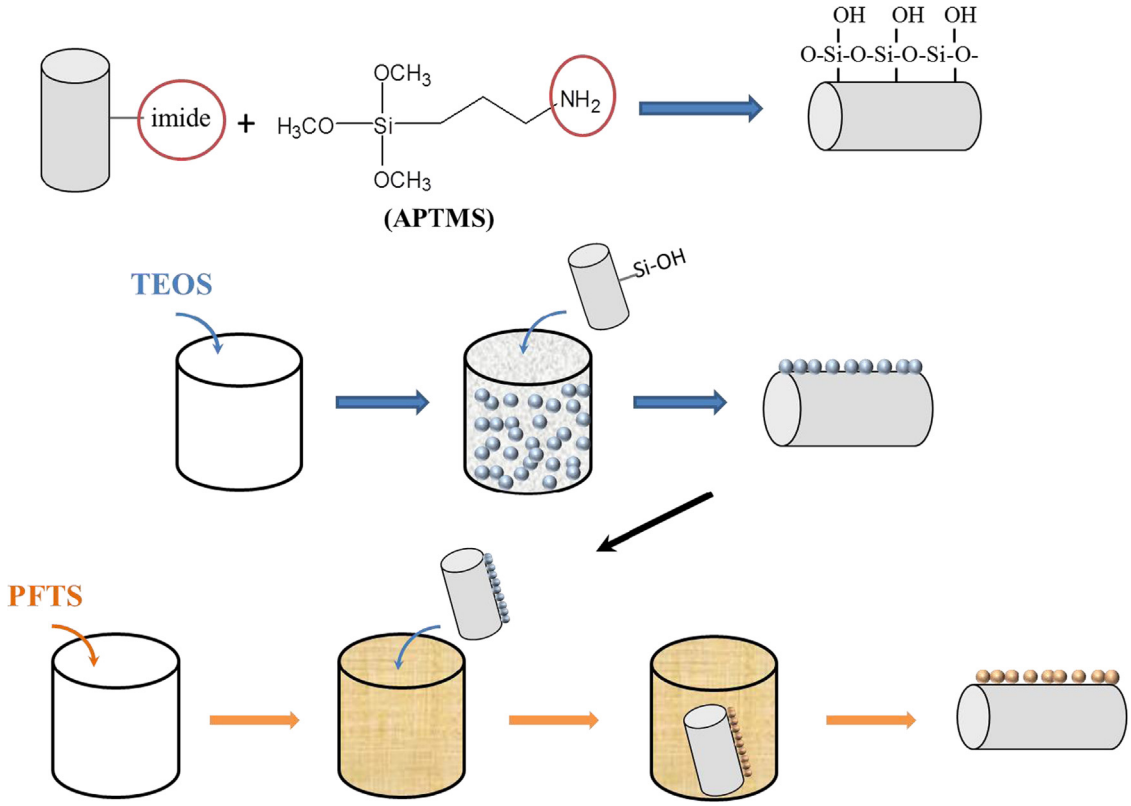

Fig. 2. Reaction route of forming the PEI-fSiO_2 organic–inorganic composite membranes.

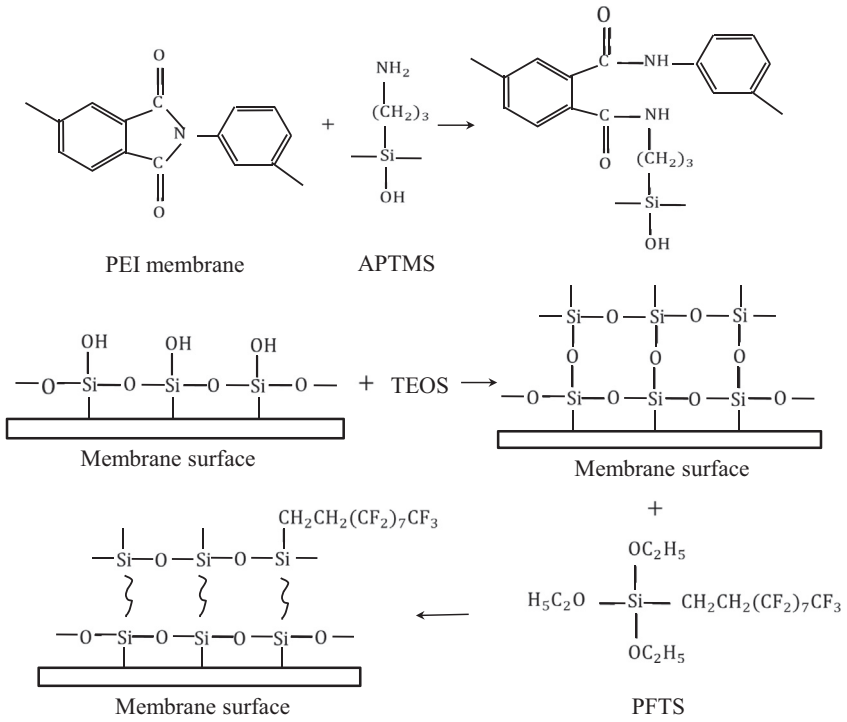

Fig. 3. Mechanism of forming the PEI-fSiO_2 organic–inorganic composite membranes.

5 kV. The membrane samples were broken in liquid nitrogen and then sputtered with a thin layer of gold using an EMITECH SC7620 sputter coater prior to analysis.

2.4.2. Membrane pore size and overall membrane porosity

The membrane pore size was measured by a capillary flow porometer (CFP 1500A, from Porous Material. Inc. (PMI)). The membrane samples were fixed into the sample holder and immersed in a liquid (Galwick) till the samples were completely wetted. Galwick has a surface tension of 16.0×10^{-3} N/m. During the test, the gas flow rate was increased stepwise and passed through the saturated sample until the applied pressure exceeded the capillary attraction of the liquid in the pores. By comparing the gas flow rates of a wet and dry sample at the same pressures, the percentage of flow passing through the pores larger than or equal to the specified size can be calculated from the pressure–size relationship [17].

The overall membrane porosity (ε), defined as the volume of the pores divided by the total volume of the membrane, was measured using a method based on the density measurements [18,19]. The equation of calculating ε is shown below

$$\varepsilon = \left(1 - \frac{\rho_{membrane}}{\rho_{PEI}}\right) 100\% \quad (2)$$

where $\rho_{membrane}$ is the density of the membrane and ρ_{PEI} is the density of the PEI powder. The $\rho_{membrane}$ is calculated by membrane weight and volume. Membrane weight was determined by an analytical balance. The membrane volume was calculated according to the inner/outer diameters and the length of the fiber sample. The ρ_{PEI} is taken as 1.27 g/cm^3. An average value of the three times of test results was considered as the overall membrane porosity.

2.4.3. Pure water permeability (PWP) test

Pure water permeability (PWP) test was performed to characterize the as-spun PEI membranes. The experiment was carried out in a cross flow filtration setup. Mili-Q ultrapure water was circulated to test the pure water flux at a constant pressure of 0.1 MPa. PWP was measured after 1 h of starting the test to eliminate the influence of membrane compaction on flux measurement.

2.4.4. Membrane chemical structure analysis

The membrane chemical structures were examined by ATR-FTIR spectra, respectively. ATR-FTIR spectra were collected at room temperature over a scanning range of 650–4000 cm^{-1} with a resolution of 4.0 cm^{-1}, using an IR Presitige-21 FT-IR (Shimadzu, Japan). The spectrometer was installed with a deuterated triglycine sulfate doped with a L-analine (DLATGS) detector and KBr beamsplitter. Spectral analysis was performed using FT-IR software (IR Solution, Shimadzu).

2.4.5. Membrane surface roughness analysis

The membrane surface morphology and roughness were analyzed by AFM XE-100 (Park System). The membrane surfaces were imaged in a scan size of 5 μm × 5 μm. The surface roughness parameters of the membranes which are expressed in terms of the mean roughness (R_a), and the root mean square of the Z data (R_q).

2.4.6. Surface hydrophobicity and mechanical properties of the composite membranes

A tensiometer (DCAT11 Dataphysics, Germany) was used to perform the dynamic contact angle measurement to determine the surface hydrophobic properties of the fibers. A sample fixed by the sample holder was hung from the arm of an electro-balance, and then experienced a cycle of immersion into DI water and successive emersion. The weight difference was continuously recorded by the electro-balance during the above loop at an interfacial moving rate of 0.2 mm/min and an immersion depth of 5 mm. Three immersion/emersion cycles were carried out for each specimen, and each run was repeated three times for all the hollow fiber samples to confirm the reproducibility within the statistical deviation. The contact angle was calculated from the wetting force based on the Wihelmy method.

Mechanical stability of the membrane was tested by an Instruon 5542 tensile test machine. The tensile modulus, tensile strength, strain at tensile strength, stress at break and strain at break were tested to indicate the membrane's mechanical strength and the degree of deformation that could be expected under a given load. The test was carried out at room temperature and 75% humidity.

2.5. Gas–liquid membrane contactor experiments

The PEI-fSiO_2 composite hollow fiber membranes were subjected to the CO_2 absorption test in a gas–liquid membrane contactor. The fibers were assembled into the PTFE modules. The characteristics of the membrane contactor modules are given in Table 2. Pure CO_2 was employed as the feed gas and the pure water or a 2 M sodium taurinate aqueous solution was used as the liquid absorbents to measure the CO_2 absorption flux. The liquid passed through the shell side and the gas flowed counter-currently through the lumen side of the hollow fibers, as the hydrophobic layers of the composite membranes were in the outer surfaces. Experimental data were recorded after the contactor system was stabilized. The detailed experimental setup and test procedures could be found elsewhere [15].

3. Results and discussion

3.1. Concept of preparing the porous PEI substrate using the triple-orifice spinneret

Two approaches can be used to obtain an open and porous skin layer of the membrane. One approach is to use a very low polymer composition in the dope solution. The drawback is that the dope viscosity would be too low to make the spinning process feasible or make the resultant membranes full of macrovoids and result in poor mechanical property. Another approach is to induce delayed liquid–liquid demixing. For the delayed demixing, the intrusion of non-solvent to the dope matrix is hindered, thus the membrane skin becomes open and porous and the macrovoids are significantly reduced. Applying a coagulant bath composing of solvent and nonsolvent mixture could a possible method to induce the delayed demixing [12,20,21]. However, this method would consume a large amount of solvent which is not feasible in the practical membrane fabrication. Moreover, it is not environmentally friendly and also imposes potential health effect as the coagulant bath is usually open to the atmosphere.

The approach of using the triple-orifice spinneret with solvent and dope co-extrusion from the spinneret simultaneously can be adopted. Firstly, the solvent contact with the outer layer of the dope effectively reduces the polymer concentration, but has no impact on the bulk dope system. Secondly, after the two-phase flow entering the coagulant bath, the outward diffusion of the solvent hinders the non-solvent inward diffusion and hence slows down the solvent and non-solvent exchange process, resulting in the delayed demixing process. The resultant membrane is expected to exhibit a very open and porous skin layer which is able to decrease the mass transfer resistance significantly, as shown in SEM images which will be discussed in the next session.

Table 2
Characteristics of the membrane contactor module.

Module ID (mm)	6.4
Module length (cm)	25
Fiber OD (mm)	1
Fiber ID (mm)	0.7
Effective fiber length (cm)	16
Effective contact area (cm^2)	20
Number of fibers	4

3.2. Characterizations of the PEI hollow fiber substrates

The SEM images of the two as-spun PEI substrates, e.g. PEI A and PEI B are shown in Fig. 4. PEI A was spun by using the standard dry-jet wet spinning process without solvent flowing in the outer channel of the spinneret. PEI B was spun with solvent phase extruding from the spinneret simultaneously with the dope solution. The dope of PEI A went through an air gap after extruded from the spinneret and entered the water bath. A relatively dense skin layer was formed. When NMP was applied in the outer orifice, an extremely open and porous skin layer with a lacy structure was obtained for PEI B. This was because the solvent in the outer channel of the spinneret reduced the outer layer polymer concentration of the dope solution and also hindered the solvent

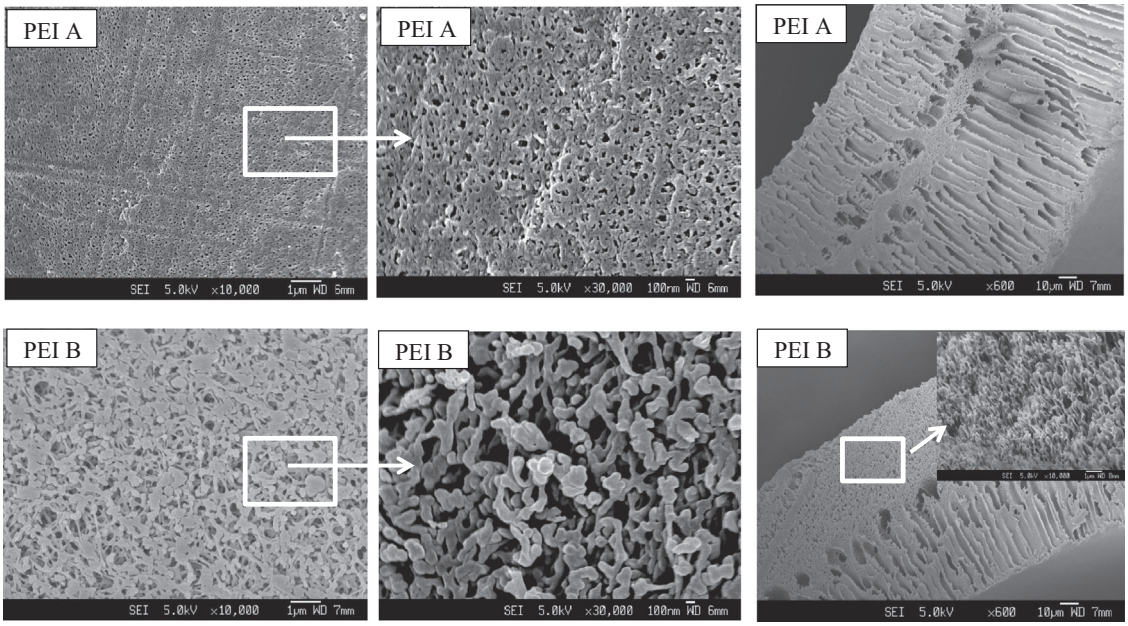

Fig. 4. SEM images of the surface and cross-section of the PEI A and PEI B substrates. Surface: left 10,000 ×, middle 30,000 × and cross section: right 600 ×.

Table 3
Characteristics of the PEI hollow fiber substrates.

Properties	PEI A	PEI B
Fiber OD (mm)	1042	966
Fiber ID (mm)	736	737
Fiber wall thickness (μm)	153	115
Surface pore size (μm)	0.03	0.09
Overall porosity (%)	81.2	71.2
PWP (L/m^2 h MPa)	6620	6650

exchange process with the external coagulant (water), resulting in a loose and open cellular structure in the skin layer.

The cross section of PEI A and PEI B are also shown in Fig. 4. For PEI A, it can be seen the finger-like structures were developed simultaneously beneath the inner and outer surfaces of the fibers with a thin layer of sponge structure sandwiched in between. This was because of the fast solvent and nonsolvent exchange process so that the dope system gelled and solidified immediately after immersion in the water bath which resulted in a membrane with a fine pore skin and finger-like pore structure. On the other hand, the substrate beneath the outer skin layer of the PEI B showed a free and interconnected pore structure. This was because the solvent flowing at the outer layer of the dope solution hindered the inward diffusion of the nonsolvent, leading to the delayed demixing which made the morphology completely different from that of PEI A. It is worth mentioning that the open cellular surface morphology would effectively reduce the mass transfer resistance, and meanwhile, it also played an important role in the SiO_2 NPs incorporation as the NPs were able to be embedded deeply in this type of morphology so that the membrane would hold the NPs through both chemical and physical interactions.

The characteristics of the as-spun PEI A and PEI B substrates in terms of fiber dimension, average pore size, overall membrane porosity and PWP are summarized in Table 3. Under the same spinning condition, the thickness of PEI B was 25% less than PEI A. The PEI B showed the pore size of 0.09 μm and PEI A showed the pore size of 0.03 μm. The PEI B exhibited smaller overall membrane porosity because of the replacement of finger-like structures and macrovoids by the interconnected pores. The PWP was almost the same for PEI A and PEI B. This was possibly because of the balance between an increased pore size and decreased overall membrane porosity of PEI B.

3.3. Membrane chemical structure analysis

The chemical structures of the original PEI membrane, APTMS treated PEI membrane, SiO_2 incorporated PEI and $fSiO_2$ incorporated PEI composite membranes were examined by ATR-FTIR. The spectra of the original PEI and APTMS treated PEI membranes have been illustrated in Zhang et al. [15]. The imide group reacted with the amine from APTMS and hence the hydroxide group was imparted on the membrane surface. The spectra of the PEI-SiO_2 and PEI-$fSiO_2$ composite membranes are shown in Fig. 5. The peak at 1719 cm^{-1} was the typical imide band corresponded to the symmetric C=O stretching of the original PEI membrane. An intense band vibrating at 1150–1000 cm^{-1} in both spectra was due to the siloxane asymmetric stretching of Si–O–Si or Si–O–R groups (R is a hydrocarbon such as –CH_2CH_3) [22], indicating the successful deposition of the SiO_2 layer on the membrane surface. The broad band in PEI-SiO_2 membrane at 3000–3600 cm^{-1} was attributed to the stretching of O–H group from the hydrophilic SiO_2 NPs. The PEI-$fSiO_2$ membrane showed a less intense O–H stretching due to the coverage of the PFTS layer on top of the SiO_2 NPs. The peak at 1199 cm^{-1} of the PEI-$fSiO_2$ membrane was assigned to the C–F stretching from the PFTS layer.

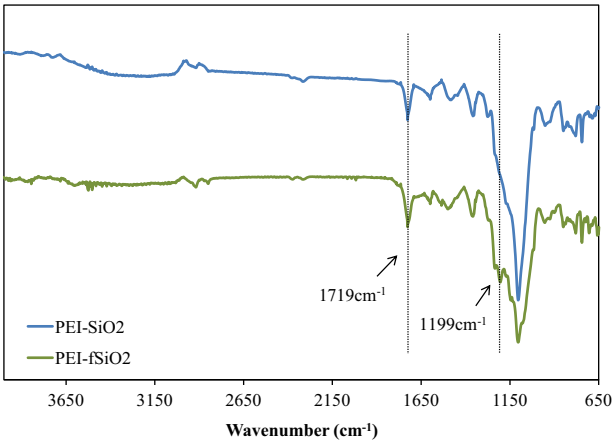

Fig. 5. ATR-FTIR spectra of the PEI-SiO_2 and PEI-$fSiO_2$ composite hollow fiber membranes.

3.4. Membrane morphology observation and surface roughness analysis

Fig. 6 shows the SEM images of the two PEI substrates after APTMS treatment and $fSiO_2$ incorporation. The nanostructured architecture can be observed clearly on the PEI A-$fSiO_2$ and PEI B-$fSiO_2$ membrane surfaces after the incorporation of $fSiO_2$ NPs on the PEI substrates. For PEI A, the surface was denser compared with PEI B and the $fSiO_2$ NPs deposited individually on top of the membrane surface. While for PEI B, the surface was so loose with cellular morphology that the $fSiO_2$ NPs were embedded into the skin layer of the membrane so that the bonding force between the NPs and membrane substrate was expected to be stronger, as the membrane was able to bond with the NPs through both chemical and physical interactions. Moreover, the deposition of $fSiO_2$ NPs was found more uniform on the PEI B surface as observed from the higher magnification surface morphology images. In addition, the skin layer cross section images of PEI B-$fSiO_2$ are also shown in Fig. 6. The embedment of the $fSiO_2$ NPs in the top skin layer of the PEI B-$fSiO_2$ can be observed from the cross section images.

The three-dimensional surface images and surface roughness parameters of the PEI membranes before and after $fSiO_2$ incorporation can be observed in Fig. 7 and Table 4. Roughness parameters, the mean roughness (R_a) defined as the arithmetic average of the absolute values of the surface height deviations measured from the center plane, and the root mean square roughness (R_q) representing the standard deviation from the mean surface plane were obtained with the AFM analysis software. Comparing with the two as-spun substrates, apparently the PEI B showed a much higher roughness due to the cellular surface morphology. After the $fSiO_2$ incorporation, the membrane PEI A-$fSiO_2$ exhibited enhanced roughness due to the nanostructured architecture on the membrane surface resulted from the presence of $fSiO_2$ NPs. It is worth mentioning the roughness of the PEI B-$fSiO_2$ became smaller compared with the PEI B. This was possibly because embedding the NPs may partially fill the holes of the membrane surface, thus reduced the roughness.

3.5. Surface hydrophobicity of the composite membranes

The membrane surface wettability was indicated by the dynamic contact angle measurement. Table 5 shows the dynamic contact angle results of the PEI membrane before and after $fSiO_2$ incorporation. We can see that for the first cycle advancing value, the PEI B (109.9 ± 1.4) was higher than the PEI A (86.2 ± 1.1) due to

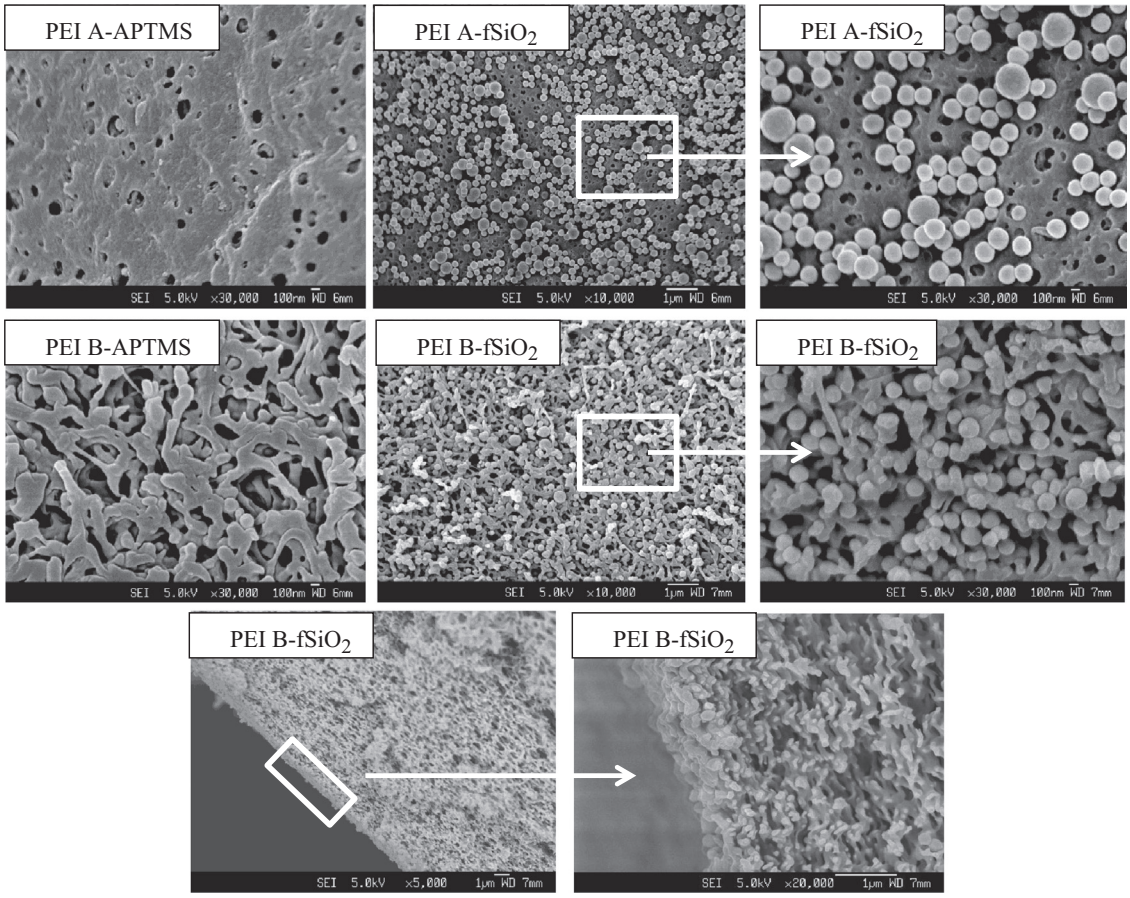

Fig. 6. SEM images of the PEI A and PEI B membranes after APTMS treatment (surface, enlarged at 30,000 ×) and $fSiO_2$ NPs incorporation (surface, enlarged at 10,000 × and 30,000 × and cross section, enlarged at 5000 × and 20,000 ×).

the higher surface roughness of the PEI B which has been demonstrated in Table 4. However, the PEI B was getting wetted quickly as indicated by the second and third cycle advancing values which dropped significantly and even became lower than that of the PEI A. This was believed to be caused by the large pore sizes in the skin layer of the PEI B, where water could enter easily and wet the surface. After the SiO_2 NPs were incorporated and hydrophobicially treated, the contact angles of the membranes behaved in a different way. It can be seen that the second and third cycle advancing contact angles were almost the same as the first cycle for both PEI A-$fSiO_2$ and PEI B-$fSiO_2$ which indicated the membranes were highly hydrophobic and kept completely dry after immersing in the water.

Based on the second cycle values, both PEI A and PEI B membrane showed an increase in advancing and receding contact angles of more than 50° because of the nanostructured architecture generated by $fSiO_2$ NPs and highly hydrophobic fluorocompounds of PFTS on the membrane surface. In particular, the PEI B-$fSiO_2$ showed a higher advancing contact angle of $123.2 \pm 0.7°$ (62° increment) and a receding contact angle of $107.2 \pm 3.9°$ (59° increment) due to the greater surface roughness. The difference between advancing and receding contact angles is called contact angle hysteresis. A high advancing/receding contact angle and low contact angle hysteresis is responsible for the low wettability of a material surface [23]. The contact angle hysteresis here was calculated according the second cycle advancing and receding contact angles. The PEI B-$fSiO_2$ showed a very low contact angle hysteresis of $15.9 \pm 4.5°$. The inherently hydrophobic membrane PVDF was prepared according to Loh et al. [24] and the contact angle values were also tested. The newly developed PEI-$fSiO_2$ membranes showed significantly higher values than PVDF membranes in all contact angle categories.

3.6. Mechanical properties of the composite membranes

Table 6 shows the mechanical properties of the PEI membranes before and after $fSiO_2$ NPs incorporation in terms of tensile modulus, stress at break and strain at break. The PEI B showed tensile modulus of 233.7 ± 14.3, which was significantly higher than that of the PEI A (116.9 ± 7.8). A high tensile modulus suggests a high rigidity of the membrane. The stress at break and strain at break of the PEI B reached 10.4 ± 0.2 and 49.4 ± 3.6, as compared to 5.4 ± 0.1 and 21.1 ± 2.1 of the PEI A, respectively. The combination of high tensile strength and strain at tensile strength makes the membrane have a high toughness. The PEI B had higher rigidity, toughness and elongation properties than that of the PEI A, which was attributed to its more interconnected pore structure, while the PEI A had a finger-like pore structure and macrovoids on it cross section. On the other hand, due to the incorporation of inorganic NPs on the PEI substrate, the composite PEI membranes showed higher rigidity but less elongation properties compared with the as-spun substrates, which was attributed to the intrinsic brittle property of inorganic materials.

3.7. Gas–liquid membrane contactor performance for CO_2 absorption

3.7.1. CO_2 absorption in gas–liquid membrane contactor

The PEI A-$fSiO_2$ and PEI B-$fSiO_2$ fibers were tested for CO_2 absorption in a gas–liquid membrane contactor. The CO_2 absorption flux with the change of the liquid velocity is shown in Fig. 8.

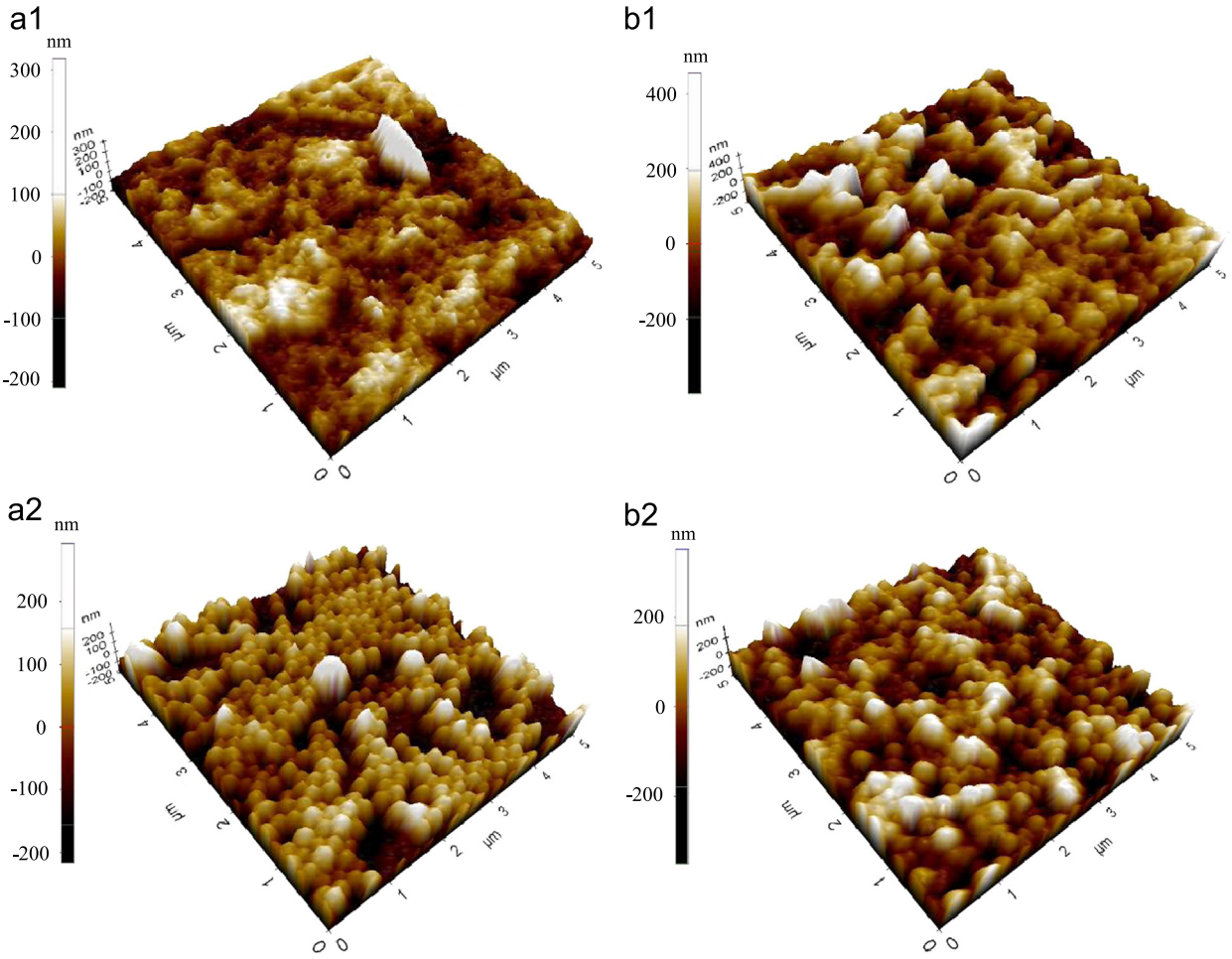

Fig. 7. Three-dimensional topography AFM images of (a1) PEI A; (b1) PEI B; (a2) PEI A-fSiO$_2$ and (b2) PEI B-fSiO$_2$ membrane.

Table 4
Surface roughness parameters of the PEI membranes before and after fSiO$_2$ incorporation.

Membrane code	Roughness	
	R_a (nm)	R_q (nm)
PEI A	35.80	50.58
PEI B	79.12	99.87
PEI A-fSiO$_2$	64.99	79.91
PEI B-fSiO$_2$	72.92	92.08

Table 5
Dynamic contact angles of PEI membrane before and after fSiO$_2$ incorporation.

Membrane code	Contact direction	First cycle (deg)	Second cycle (deg)	Third cycle (deg)	Contact angle hysteresis (deg)
PEI A	Advancing	86.2 ± 1.1	70.7 ± 2.5	70.4 ± 2.7	23.2 ± 4.1
	Receding	47.6 ± 1.5	47.5 ± 1.6	47.6 ± 1.7	
PEI B	Advancing	109.9 ± 1.4	60.8 ± 1.7	58.3 ± 3.1	12.7 ± 2.5
	Receding	48.0 ± 1.0	48.1 ± 0.8	48.2 ± 0.9	
PEI A-fSiO$_2$	Advancing	121.0 ± 2.0	121.0 ± 2.1	120.8 ± 2.2	22.3 ± 3.3
	Receding	98.2 ± 1.0	98.7 ± 1.1	98.7 ± 1.5	
PEI B-fSiO$_2$	Advancing	123.2 ± 1.3	123.2 ± 0.7	123.2 ± 0.7	15.9 ± 4.5
	Receding	106.1 ± 3.9	107.2 ± 3.9	107.1 ± 3.8	
PVDF	Advancing	92.3 ± 3.7	89.8 ± 5.1	89.2 ± 5.0	32.6 ± 7.4
	Receding	57.6 ± 2.6	57.2 ± 2.3	57.2 ± 2.4	

Table 6
Mechanical properties of PEI membrane before and after fSiO$_2$ incorporation.

Membrane code	Young's modulus (MPa)	Stress at break (MPa)	Strain at break (%)
PEI A	116.9 ± 7.8	5.4 ± 0.1	21.1 ± 2.1
PEI B	233.7 ± 14.3	10.4 ± 0.2	49.4 ± 3.6
PEI A-fSiO2	125.6 ± 5.7	5.5 ± 0.1	11.3 ± 0.4
PEI B-fSiO2	274.9 ± 16.2	10.6 ± 0.1	19.2 ± 1.0

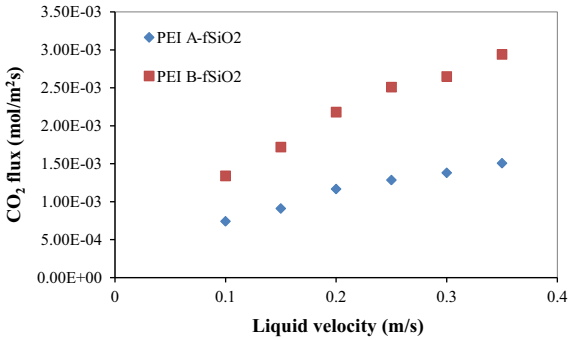

Fig. 8. CO_2 flux using pure water as the absorbent (atmospheric pressure, absorbent temperature: 298.15 K, gas velocity 0.12 m/s).

Pure CO_2 and pure water was used in this experiment. It can be observed that the CO_2 flux increased with the increase in the water flow rate. This is a well-known behavior in membrane

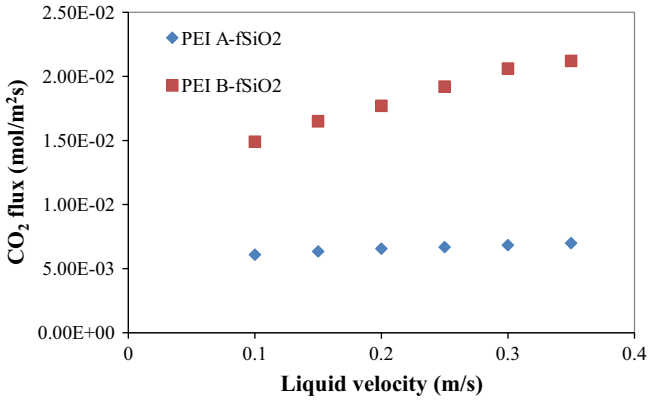

Fig. 9. CO_2 flux using 2 M taurinate sodium as the absorbent (atmospheric pressure, absorbent temperature: 298.15 K, gas velocity 0.8 m/s).

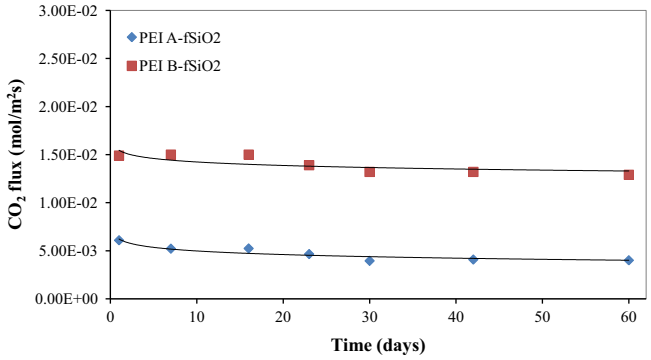

Fig. 10. Long term CO_2 flux using 2 M taurinate sodium as the absorbent (atmospheric pressure, absorbent temperature: 298.15 K, gas velocity 0.8 m/s).

contactor which indicates the main resistance exists in the liquid phase in the case of physical absorption of CO_2 [1,25,26]. The change in gas velocity hardly affected the absorption performance. As can be seen from Fig. 8, the PEI B-$fSiO_2$ possessed much higher CO_2 flux than that of the PEI A-$fSiO_2$. At a liquid velocity of 0.3 m/s, the PEI A-$fSiO_2$ showed the CO_2 flux of 1.38×10^{-3} mol/m^2 s while the PEI B-$fSiO_2$ showed the CO_2 flux of 2.65×10^{-3} mol/m^2 s, which was almost twice of the PEI A-$fSiO_2$'s flux. This was most likely due to the higher surface porosity and bigger pore sizes of the PEI B-$fSiO_2$ membrane which significantly reduced the mass transfer resistance. In contrast, the relatively dense skin layer of the PEI A-$fSiO_2$ imposed higher mass transfer resistance compared with the PEI B-$fSiO_2$. Moreover, the high degree of pore interconnectivity in the cross section the PEI B-$fSiO_2$ was believed to be another factor contributing to its high flux.

Fig. 9 shows the CO_2 flux of the composite PEI-$fSiO_2$ membranes by using amino acid salts as the absorbent liquid, e.g. 2 M aqueous sodium taurinate solution. The CO_2 removal absorption liquids based on amino acid salts have similar absorption characteristics as conventional alkanolamine, but they have less membrane wetting tendencies [9,27]. It is well understood that the physical absorption suffers low separation efficiency than chemical absorption. In the case of chemical absorption by using a 2 M aqueous sodium taurinate solution, the CO_2 flux of the PEI A-$fSiO_2$ was 6.83×10^{-3} mol/m^2 s at a liquid velocity of 0.3 m/s; it was four times higher than the flux in physical absorption at the same liquid velocity. While the CO_2 flux of the PEI B-$fSiO_2$ was 2.06×10^{-2} mol/m^2•, which was 6.7 times higher than the flux in physical absorption. In addition, the flux of the PEI B-$fSiO_2$ was three times of the PEI A-$fSiO_2$'s flux because of its higher surface porosity and pore interconnectivity beneath the top layer. Moreover, it is observed that with increase in the liquid velocity, the CO_2 absorption flux increased. This is because there was a significant depletion of the active sodium taurinate at the gas–liquid interface (shell side) because the instantaneous CO_2 absorption took place. An increase in the liquid absorbent velocity would accelerate the supply of fresh sodium taurinate and mitigate the depletion effectively, and therefore enhanced the mass transfer rate of CO_2 [28].

3.7.2. *Long-term performance in gas–liquid membrane contactor*

The long-term performance of CO_2 flux of the PEI A-$fSiO_2$ and PEI B-$fSiO_2$ membranes by using 2 M sodium taurinate were carried out for 60 d. Measurements were carried out periodically to observe the change in CO_2 absorption flux. The membrane contactor modules were fully immersed in the sodium taurinate solution after every experiment to ensure that the outer surfaces of the hollow fibers would be in constant contact with the absorbent. The experimental results are shown in Fig. 10. The CO_2 flux of the PEI B-$fSiO_2$ membrane was consistently higher than that of the PEI A-$fSiO_2$ membrane. Through the 60 d testing, the PEI B-$fSiO_2$ membrane was able to maintain a relatively stable performance with CO_2 flux around 1.4×10^{-2} mol/m^2 s while the flux of the PEI A-$fSiO_2$ decreased gradually from 6.0×10^{-3} mol/m^2 s to 4.0×10^{-3} mol/m^2 s, suggesting that the PEI A-$fSiO_2$ was partially wetted by the 2 M sodium taurinate solution. This was probably due to the relatively lower surface hydrophobicity of the PEI A-$fSiO_2$ membranes as compared with PEI B-$fSiO_2$. The long-term test indicated the great potential of PEI B-$fSiO_2$ membranes in the gas–liquid membrane contactor application.

3.7.3. *Comparison of CO_2 flux of various membranes used in gas–liquid membrane contactors*

Table 7 shows the summary of the CO_2 flux of various membranes used in gas–liquid membrane contactors. We can see that PEI B-$fSiO_2$ (#2) possessed superior CO_2 absorption performance over the other commonly used polymeric membranes. The surface modifying macromolecule (SMM) modified PEI hollow fiber membranes (#5) also showed a very high CO_2 flux compared with others, but the hydrophobicity was relatively low with contact angle of 95° and the long-term performance of the membrane was not available [29]. In fact, it is rare that the in house-made hollow fiber membranes experienced long-term stability investigation, in particular for such a long period of time—60 d. Both the high CO_2 flux and stable long-term performance indicated the PEI B-$fSiO_2$ hollow fiber membranes have the great potential to be used practically in the gas–liquid membrane contactor process, which also demonstrated the important role of membrane fabrication and modification techniques in facilitating the commercialization of membrane contactor technology.

4. Conclusions

Aiming to minimize the membrane mass transfer resistance, this study utilized the unique structure of triple-orifice spinneret to fabricate PEI hollow fiber membranes with a highly porous and interconnected surface structure, which is desirable for incorporating $fSiO_2$ NPs on the membrane surface. The following conclusions can be drawn from this study:

(1) The solvent-dope solution co-extrusion method using a triple-orifice spinneret for hollow fiber spinning is an effective way to increase the surface porosity, pore size and pore interconnectivity of the membrane.
(2) The membrane mechanical property was improved because of the highly porous cellular surface structure and high degree of pore interconnectivity, which is also favorable for NPs embedment.

Table 7
Overall comparison of CO_2 flux of various membranes used in membrane contactors.

Membrane	ID/OD (mm)	Pore size (μm)	Porosity (%)	CO_2 flux[a] ($mol/m^{-2}\ s^{-1}$)	Shell side	Highlights	Manufacturer	Ref.
#1 PEI	0.7/1	0.03[b]	81	1.38×10^{-3}	Water	Composite/NPs incorporated	In-house made	Current work
#2 PEI	0.7/0.9	0.09[b]	71	2.65×10^{-3}	Water	Novel spinning technique Composite/NPs incorporated	In-house made	Current work
#3 PEI	0.8/1.1	0.04[b]	-	8.68×10^{-4}	Water	Composite/NPs incorporated	In-house made	[15]
#4 PEI	0.3/0.6	0.05	77	1.2×10^{-3}	CO_2	Pristine PEI	In-house made	[29]
#5 PEI	0.35/0.6	0.07	81	2.3×10^{-3}	CO_2	SMMs modified		
#6 PVDF	0.3/0.4	MWCO 290 kDa	76	1.0×10^{-3}	Water	Phosphorous acid as the additive	In-house made	[7]
#7 PVDF	–/–	–	–	8.0×10^{-4}	Water	Commercial	Tianjin Motian Membrane	
#8 PVDF	0.3/0.5	MWCO 40 kDa	–	8.0×10^{-4}	Water	Pristine PVDF	In-house made	[30]
#9 PVDF	0.65/1	0.2	75	6.5×10^{-4} (extrapolated)	CO_2	Commercial	Memcor Australia	[31]
#10 PAI	1.1/1.4	MWCO 20 kDa[b]	72	8.5×10^{-4}	Water	APTMS & FS10 modified	In-house made	[32]
#11PSf	0.5/1	0.01	72	7.5×10^{-4}	CO_2	Glycerol as the additive	In-house made	[4]
#12 PP	0.22/0.23	0.04	40	1.4×10^{-3}	CO_2	Commercial	Celgard Inc.	[28]

[a] Achieved at liquid velocity of 0.3 m/s.
[b] Pore size/porosity of the polymeric membrane substrate.

(3) The incorporation of $fSiO_2$ NPs on the PEI hollow fiber membrane led to a significant improvement in surface hydrophobicity, as evidenced by the advancing contact angle value of 123.2°, receding contact angle value of 107.2°.
(4) The PEI B-$fSiO_2$ showed a significant flux enhancement and more stable long-term performance compared with the PEI A-$fSiO_2$ membrane.
(5) The highly hydrophobic composite hollow fiber membrane was able to outperform conventional polymeric membrane in term of superior gas absorption flux and outstanding long-term stability, suggesting that the formation of organic–inorganic composite membranes is an effective way to enhance the feasibility of membrane contactor processes for practical applications.

Acknowledgments

We thank Ms Yao Lei for her kind help in taking SEM images and Ms Lim Siow Kee for her kind assistance in conducting membrane contactor experiments. This research grant is supported by the Singapore National Research Foundation under its Environmental & Water Technologies Strategic Research Programme and administered by the Environment & Water Industry Programme Office (EWI) of the PUB (EWI RFP 0901-IRIS-04-06). We are also grateful to Singapore Economic Development Board for funding to Singapore Membrane Technology Centre.

References

[1] Y. Zhang, J. Sunarso, S. Liu, R. Wang, Current status and development of membranes for CO_2/CH_4 separation: a review, Int. J. Greenh. Gas Control 12 (2013) 84–107.
[2] Y. Zhang, R. Wang, Gas–liquid membrane contactors for acid gas removal: recent advances and future challenges, Curr. Opin. Chem. Eng. 2 (2013) 255–262.
[3] M. Mavroudi, S.P. Kaldis, G.P. Sakellaropoulos, A study of mass transfer resistance in membrane gas–liquid contacting processes, J. Membr. Sci. 272 (2006) 103–115.
[4] A. Mansourizadeh, A.F. Ismail, Effect of additives on the structure and performance of polysulfone hollow fiber membranes for CO_2 absorption, J. Membr. Sci. 348 (2010) 260–267.
[5] S. Wongchitphimon, R. Wang, R. Jiraratananon, Surface modification of polyvinylidene fluoride-co-hexafluoropropylene (PVDF-HFP) hollow fiber membrane for membrane gas absorption, J. Membr. Sci. 381 (2011) 183–191.
[6] A. Mansourizadeh, A.F. Ismail, M.S. Abdullah, B.C. Ng, Preparation of polyvinylidene fluoride hollow fiber membranes for CO_2 absorption using phase-inversion promoter additives, J. Membr. Sci. 355 (2010) 200–207.
[7] S. Atchariyawut, C. Feng, R. Wang, R. Jiraratananon, D.T. Liang, Effect of membrane structure on mass-transfer in the membrane gas–liquid contacting process using microporous PVDF hollow fibers, J. Membr. Sci. 285 (2006) 272–281.
[8] A.C.M. Franken, J.A.M. Nolten, M.H.V. Mulder, D. Bargeman, C.A. Smolders, Wetting criteria for the applicability of membrane distillation, J. Membr. Sci. 33 (1987) 315–328.
[9] P.S. Kumar, J.A. Hogendoorn, P.H.M. Feron, G.F. Versteeg, New absorption liquids for the removal of CO_2 from dilute gas streams using membrane contactors, Chem. Eng. Sci. 57 (2002) 1639–1651.
[10] F. Edwie, M.M. Teoh, T.-S. Chung, Effects of additives on dual-layer hydrophobic–hydrophilic PVDF hollow fiber membranes for membrane distillation and continuous performance, Chem. Eng. Sci. 68 (2012) 567–578.
[11] L. Setiawan, R. Wang, L. Shi, K. Li, A.G. Fane, Novel dual-layer hollow fiber membranes applied for forward osmosis process, J. Membr. Sci. 421-422 (2012) 238–246.
[12] P. Wang, M.M. Teoh, T.S. Chung, Morphological architecture of dual-layer hollow fiber for membrane distillation with higher desalination performance, Water Res. 45 (2011) 5489–5500.
[13] T. He, M.H.V. Mulder, M. Wessling, Preparation of porous hollow fiber membranes with a triple-orifice spinneret, J. Appl. Polym. Sci. 87 (2003) 2151–2157.
[14] S. Bonyadi, T.S. Chung, Highly porous and macrovoid-free PVDF hollow fiber membranes for membrane distillation by a solvent-dope solution co-extrusion approach, J. Membr. Sci. 331 (2009) 66–74.
[15] Y. Zhang, R. Wang, Fabrication of novel polyetherimide-fluorinated silica organic–inorganic composite hollow fiber membranes intended for membrane contactor application, J. Membr. Sci. 443 (2013) 170–180.
[16] W. Stöber, A. Fink, E. Bohn, Controlled growth of monodisperse silica spheres in the micron size range, J. Colloid Interface Sci. 26 (1968) 62–69.
[17] X. Yang, R. Wang, L. Shi, A.G. Fane, M. Debowski, Performance improvement of PVDF hollow fiber-based membrane distillation process, J. Membr. Sci. 369 (2011) 437–447.
[18] Y. Tang, N. Li, A. Liu, S. Ding, C. Yi, H. Liu, Effect of spinning conditions on the structure and performance of hydrophobic PVDF hollow fiber membranes for membrane distillation, Desalination 287 (2012) 326–339.
[19] J. Xu, Z.L. Xu, Poly(vinyl chloride) (PVC) hollow fiber ultrafiltration membranes prepared from PVC/additives/solvent, J. Membr. Sci. 208 (2002) 203–212.
[20] M.M. Teoh, T.S. Chung, Membrane distillation with hydrophobic macrovoid-free PVDF-PTFE hollow fiber membranes, Sep. Purif. Technol. 66 (2009) 229–236.
[21] S. Bonyadi, T.S. Chung, R. Rajagopalan, A novel approach to fabricate macrovoid-free and highly permeable PVDF hollow fiber membranes for membrane distillation, AIChE J. 55 (2009) 828–833.
[22] A. Irzh, L. Ghindes, A. Gedanken, Rapid deposition of transparent superhydrophobic layers on various surfaces using microwave plasma, ACS Appl. Mater. Interfaces 3 (2011) 4566–4572.
[23] X.M. Li, D. Reinhoudt, M. Crego-Calama, What do we need for a superhydrophobic surface? A review on the recent progress in the preparation of superhydrophobic surfaces, Chem. Soc. Rev. 36 (2007) 1350–1368.
[24] C.H. Loh, R. Wang, Effects of additives and coagulant temperature on fabrication of high performance PVDF/pluronic F127 blend hollow fiber membranes via nonsolvent induced phase separation, Chin. J. Chem. Eng. 20 (2012) 71–79.
[25] S. Atchariyawut, R. Jiraratananon, R. Wang, Separation of CO_2 from CH_4 by using gas–liquid membrane contacting process, J. Membr. Sci. 304 (2007) 163–172.
[26] Y. Zhang, R. Wang, L. Zhang, A.G. Fane, Novel single-step hydrophobic modification of polymeric hollow fiber membranes containing imide groups:

its potential for membrane contactor application, Sep. Purif. Technol. 101 (2012) 76–84.
[27] P.H.M. Feron, A.E. Jansen, Capture of carbon dioxide using membrane gas absorption and reuse in the horticultural industry, Energy Convers. Manage. 36 (1995) 411–414.
[28] H.Y. Zhang, R. Wang, D.T. Liang, J.H. Tay, Theoretical and experimental studies of membrane wetting in the membrane gas–liquid contacting process for CO_2 absorption, J. Membr. Sci. 308 (2008) 162–170.
[29] G. Bakeri, A.F. Ismail, D. Rana, T. Matsuura, Development of high performance surface modified polyetherimide hollow fiber membrane for gas–liquid contacting processes, Chem. Eng. J. 198–199 (2012) 327–337.
[30] C. Feng, R. Wang, H. Zhang, L. Shi, Diverse morphologies of PVDF hollow fiber membranes and their performance analysis as gas/liquid contactors, J. Appl. Polym. Sci. 119 (2011) 1259–1267.
[31] S. Atchariyawut, R. Jiraratananon, R. Wang, Mass transfer study and modeling of gas–liquid membrane contacting process by multistage cascade model for CO_2 absorption, Sep. Purif. Technol. 63 (2008) 15–22.
[32] Y. Zhang, R. Wang, S. Yi, L. Setiawan, X. Hu, A.G. Fane, Novel chemical surface modification to enhance hydrophobicity of polyamide–imide (PAI) hollow fiber membranes, J. Membr. Sci. 380 (2011) 241–250.